Proceedings of the 29th Annual International
Conference of the IEEE EMBS
Cité Internationale, Lyon, France
August 23-26, 2007.

ThB13.4

Virtual Thermistor

Jin Fei
Computational Physiology Lab
Department of Computer Science
University of Houston
Houston, Texas 77204–3010

jinfei@cs.uh.edu

Ioannis Pavlidis
Computational Physiology Lab
Department of Computer Science
University of Houston
Houston, Texas 77204–3010

ipavlidis@uh.edu

Abstract— **The present paper unveils a methodology to recover the breathing signal from the subject's nostrils through thermal imaging. The resulting functionality is equivalent to that of a thermistor, but it is materialized in a contact-free manner. First, the nostril region is segmented and it is tracked over time through coalitional tracking. The mean thermal signal of the nostril region carries the breathing information. This information is extracted through wavelets analysis. The method has been tested on 20 healthy individuals. The frequencies of the breathing signals determined via the imaging computation were compared with those of the corresponding signals acquired with thermistors. The high degree of agreement between the two measurement methods confirms the validity of the proposed approach and opens the way for clinical applications.**

I. INTRODUCTION

Breath analysis plays an important role in the diagnosis and management of respiratory diseases like sleep obstructive apnea, bronchitis, and asthma. In fact, breathing rate is one of the vital signs and hence, indicative of the overall health status of a subject. The normal breathing rate of resting adults varies from $12 - 18$ cycles per minute (cpm) [1]. Human breathing consists of expiration and inspiration phases. The expiration phase has higher temperature than the inspiration phase [2][3].

Various types of contact modalities have been developed to measure human breathing rate. The respiratory belt transducer measures the breathing rhythm via pressure changes on the strap sensor fitted on the subject's chest or abdomen [4]. The nasal thermistor measures nasal air temperature variation as an indication of respiration [5]. The thermistor probe has to be secured in front of the nostrils.

The first non-contact breathing rate measurement method was introduced by Greneker et al. [6] and is based on active sensing. It is called Radar Vital Signs Monitor (RVSM) and is able to measure the subject's heart beat and breathing rate at distances up to $30\ ft$. It senses the chest wall moving up and down during breathing by Doppler modulated radar. The RVSM measurements are sensitive to small body movement.

Thermal infrared imaging is a passive contact-free modality. In previous publications we have demonstrated that thermal imaging can be used to measure various physiological variables, including blood flow [7], heart rate [8], and breathing rate [9][10]. In fact, it is an ideal modality for sustained physiological monitoring [11].

In [9] we demonstrated for the first time the feasibility of breath rate measurement through thermal imaging. Specif-ically, we proposed a statistical methodology that models breathing as a mixture of expiration and non-expiration distributions. Every frame is classified as expiratory or non-expiratory by comparing the incoming distributions with the existing distributions using the Jeffrey's divergence measure. Thanks to this frame labeling we are able to compute the breathing rate. In [10] we retrofitted the thermal imaging sensor with an optical band-pass filter in the CO_2 absorption zone to improve the signal to noise ratio. Then, we proceeded to compute the breathing rate using Fourier instead of statistical analysis.

In this paper, we introduce a new and improved breathing rate measurement method based on automatic tracking/localization of the nasal region and wavelet analysis. No band-pass optical filtering is necessary. In section II we describe the tracking and localization algorithms as well as the wavelet-based signal extraction method. We discuss the experimental setup in section III-A and present the experimental results in section III-B. Section IV concludes the paper.

II. METHODOLOGY

To measure the breathing rate in thermal video we need to track the motion of subject, localize the measurement region, and analyze the extracted thermal signal. We address each of these issues in detail in the following subsections.

A. Tracking Region of Interest

We chose the coalitional tracking algorithm [12] for breath analysis. It optimizes multi-tracker interaction via game theory. We used a coalition grid composed of four CONDENSATION trackers [13] (see Fig. 1).The CONDENSATION algorithm contains statistical prediction and evaluation phases.
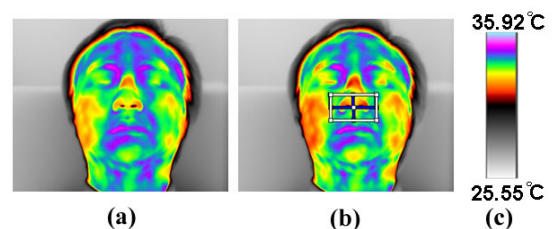

Fig. 1. (a) Thermal snapshot of a subject's face. (b) Initialization of coalitional tracker. (c) Thermal color map.

B. Localizing Region of Interest

The measurement region of interest (MROI) for breathing is the nostrils. This region features both spatial and temporal variances. First, the shape of the nostril region is different for different individuals. Thermal imaging is a functional image modality that records the changing image physiology. In the case of breathing, thermal imagery registers the temperature fluctuation between the inspiration and expiration phases. This, however, increases the segmentation difficulty, as the shape of nostrils varies temporally due to the varying thermal signature of inspiration and expiration. (see Fig. 2).
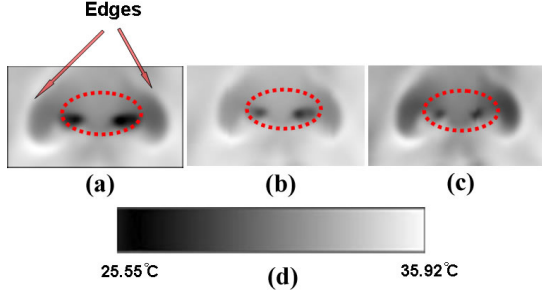

Fig. 2. Temporal variance of nostril region in thermal imagery during breathing. (a) Inspiration phase. (b) Transition phase. (c) Expiration phase. (d) Thermal color map.

Fig. 2 shows the nostrils being separated from the rest of the facial tissue due to colder boundaries formed by cartilage. This feature can help to localize MROI. We use the horizontal gradients to detect the left and right edges of the nostrils and the vertical gradients to detect the nose base. We obtain the horizontal $H(x)$ and vertical $V(y)$ projection profiles of nasal tissue by averaging pixel intensities column- and row-wise in the thermal image. We obtain the left and right nostril edges by locating the left- and right-most peaks of $H(x)$. We obtain the base edge of nose by locating the highest peak of $V(y)$ (see Fig. 3).

The MROI selection varies from frame to frame. Fig. 4 (a) and (c) show the horizontal and vertical nostril projections along the timeline for a typical subject. Some projections are weak and the locations vary as well. We use a time window of 200 frames to compute the mean horizontal and vertical projections in Fig. 4 (b) and (d) correspondingly. This time window is representative of the full spatiotemporal evolution, as it covers both an expiration and inspiration phases.

Based on anthropometric knowledge we divide the distance between left and right nostril edges by 3 and use this as an estimate of the nostrils' height (see Fig. 5).

Once the nostril region is localized, we compute the mean temperature within MROI in every frame. This produces a quasi-periodic thermal signal along the timeline, which is indicative of the breathing function.

C. Wavelet Analysis

We perform identical wavelet analysis on the extracted imaging and thermistor nasal signals to recover the breathing rate. Thus, suffice to present the imaging nasal signal analysis only. Wavelets is the appropriate analysis tool as breathing
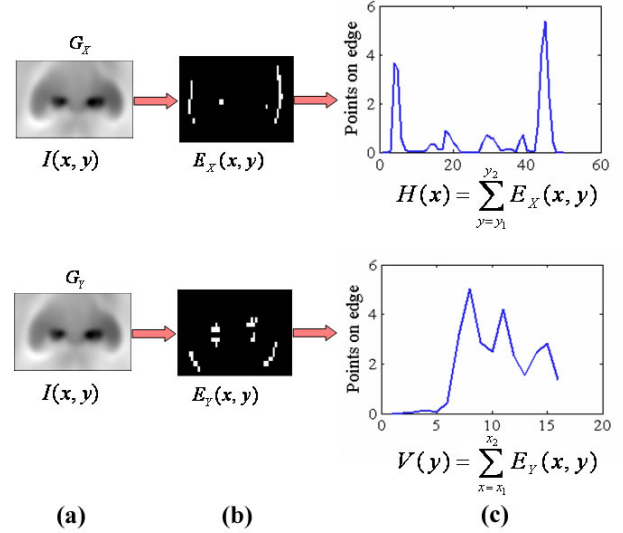

Fig. 3. Top: Determination of left and right nostril edges. Bottom: Determination of base edge. (a) MROI images. (b) Edge images. (c) Integral projections.
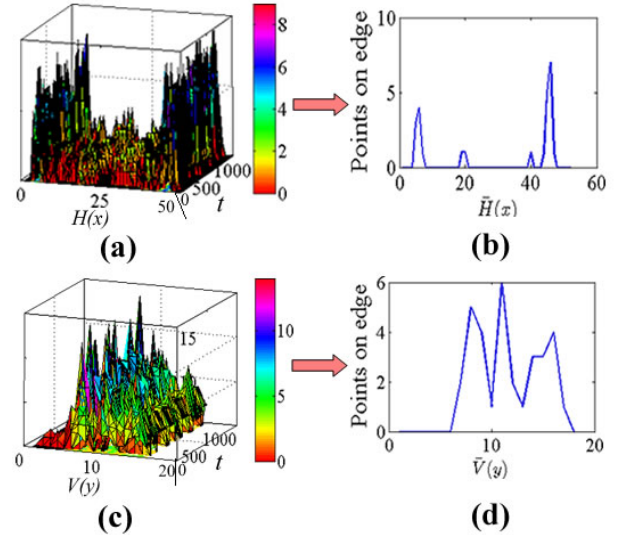

Fig. 4. Spatiotemporal evolution of integral nostril projections for a typical subject. (a) Horizontal projections along time. (b) Mean horizontal integral projection. (c) Vertical projections along time. (d) Mean vertical integral projection.

is a non-stationary process. The thermal video sampling rate fluctuates around 55 frames per second (fps). A constant sampling rate is necessary for optimal results in wavelet decomposition. We choose $\delta = 10 \ fps$ as the re-sampling rate of the thermal signal.

We normalize and perform wavelet analysis on sliding segments (windows) of the re-sampled thermal signal. This analysis yields the breathing rate. As the sliding window travels along the evolving timeline of the re-sampled signal, we compute a series of breathing rates. This provides the breath computation in real time. The details of each algorithmic step are as follows:
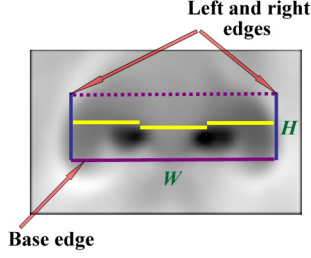
251

Fig. 5. MROI based on mean nose edges and anthropometric estimates.

1) Normalization: We define as $S(t)$, $t \in \{0, \cdots, N\}$, the re-sampled breathing signal. We normalize the signal amplitude as follows:

$$S'(t) = \frac{S(t) - \mu}{\sigma}, \qquad (1)$$

where μ and σ are the mean and standard deviation of $S(t)$ respectively. The normalization transforms signal $S(t)$ to $S'(t)$ with mean $\mu' = 0$ and standard deviation $\sigma' = 1$.

2) Wavelet Transform: We perform Continuous Wavelet Transformation (CWT) [14] on the re-sampled and normalized thermal signal:

$$\Psi_x^{\Psi}(\tau, s) = \frac{1}{\sqrt{|s|}} \int S'(t) \psi(\frac{t - \tau}{s}) dt, \qquad (2)$$

where ψ is the 'mother wavelet', τ represents the translation parameter, while s denotes the scale at which the signal is examined. We use the Mexican Hat (MH) [14] as the mother wavelet.

CWT allows analysis at all scales, hence, facilitating the extraction of the signal component of interest (i.e., breathing). We assume that the breathing component exists at a scale s_{max} corresponding to a local maximum of the wavelet energy coefficients $WT_i(t)$:

$$s_{max} = \underset{i}{argmax} \quad \{\sum |WT_i(t)|^2\}. \qquad (3)$$

Given a mother wavelet, the frequency that maximizes its transform is the center frequency F_c. The 'breathing' wavelet is dilated at scale s_{max}. Taking into account that the thermal signal has been resampled at a frequency $\delta = 10 \ fps$, the breathing rate BR is:

$$BR = \frac{F_c \cdot \delta}{s_{max}}. \qquad (4)$$

III. EXPERIMENTS

A. Experimental Setup

The center-piece of the imaging system we use in our experiments is a FLIR SC6000 Mid-Wave Infra-Red (MWIR) camera with an Indium Antimonite (InSb) detector operating in the range $3 - 5 \ \mu m$ [15]. The camera has a focal plane array (FPA) with maximum resolution of 640×512 pixels.

The sensitivity is $0.025° \ C$. The camera is outfitted with a MWIR $50mm$ lens $f/2.3$, $Si : Ge$, bayonet mount from FLIR Systems [15].

The ground-truth system is composed of a PowerLab 8/30 data acquisition system and a thermistor from ADInstruments [4]. An electronic trigger synchronizes the imaging and ground-truth systems.

The experiments took place in a climate controlled room. Subjects were located $6 \ ft$ away from the imaging system and offered a frontal view while sitting in a comfortable chair. The subjects were also fitted with the nasal thermistor to ground truth the imaging measurements. The MWIR camera was calibrated with a two-point calibration at $28° \ C$ and $38° \ C$, which are the end points of a typical temperature distribution on a human face. We recorded ~ 3 min thermal clips (and corresponding thermistor signals) for twenty (20) subjects.

B. Experimental Results

Based on the methodology described in Section II, we determine the breathing rate from the thermal imaging and thermistor signals by computing the wavelet energy curves in all scales and selecting the local maximum in the small scale region. The small scale region corresponds to relatively high frequency phenomena embedded in the signals, and breathing is one of them. Actually, it is expected to be the strongest phenomenon present due to the measurement locale. Fig. 6 shows the imaging and thermistor energy curves for the corresponding signals of a subject included in the test population. One can observe the simultaneous peaks of the two curves, which indicate agreement between the two modalities as to the scale (and thus, the frequency) of the breathing phenomenon.
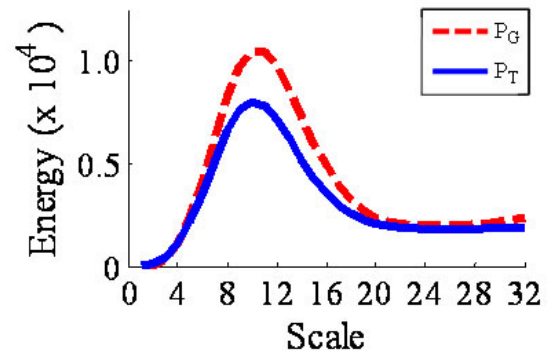

Fig. 6. Wavelet energy curves of the thermal imaging P_T and thermistor P_G signals for a subject. Only small scales [1-32] are shown.

Table I shows the detailed experimental results. The imaging measurements (BR_T) are juxtaposed with the corresponding ground-truth ones (BR_G) obtained through the thermistor.

The comparison between the two modalities is based on two measures, $CAND$ and $CuSum$. $CAND$ stands for

Subjects	$\overline{BR_G}$	$\overline{BR_T}$	$CAND(\%)$	$CuSum(\%)$
S01	12.83	12.81	99.81	13.27
S02	18.49	18.34	99.19	6.80
S03	8.22	8.33	98.68	10.37
S04	21.52	21.23	98.64	7.45
S05	20.76	21.17	98.03	6.80
S06	14.89	14.88	99.97	8.26
S07	16.56	16.68	99.26	6.88
S08	16.08	16.22	99.09	13.10
S09	15.20	14.80	97.39	11.99
S10	18.70	18.69	99.95	7.24
S11	13.55	13.22	97.54	19.54
S12	13.30	13.10	98.49	11.27
S13	13.31	13.06	98.07	13.65
S14	13.67	13.52	98.89	9.04
S15	21.65	21.88	98.92	9.46
S16	12.75	11.63	91.25	13.40
S17	16.41	16.23	98.94	6.33
S18	17.72	17.55	99.06	10.06
S19	14.50	13.99	96.48	11.25
S20	15.59	15.25	97.83	12.44
Mean	15.79	15.63	98.27	10.42

Complement of the Absolute Normalized Difference:

$$CAND = 1 - \frac{|\overline{BR_T} - \overline{BR_G}|}{\overline{BR_G}}, \qquad (5)$$

which is the absolute difference between the thermal imaging and ground-truth measurements normalized against the ground-truth and subtracted from unity. This gives a weighted indication of how close the thermal imaging measurement (BR_T) is to the ground-truth measurement (BR_G) in each case. The mean $\overline{CAND}$ for the experiment is 98.27%.

$CuSum$ stands for Cumulative Sum and is an indication of the instantaneous error in the imaging measurement with respect to the ground-truth measurement:

$$CuSum = \frac{1}{T}\sum_{t=1}^{T}\frac{|BR_T(t) - BR_G(t)|}{BR_G(t)} \times 100\%. \qquad (6)$$

The mean $\overline{CuSum}$ error for the experiment is 10.42%. On average (see $\overline{CAND}$), the two modalities give almost identical measurements. There is more discrepancy if one examines the measurements on a beat by beat basis (see $\overline{CuSum}$) , but these tend to cancel out on the whole.

IV. Conclusion

Breathing is one of the vital signs. It is used as an indicator of overall health status and also in diagnosis of chronic or acute diseases, like obstructive sleep apnea or heart attack. In this paper we have described a new method based on passive imaging to measure breathing rate. It is a step forward with respect to previous methods we reported on this matter. The present method automatically localizes the nasal region and cancels the effect of head motion. Also, a novel departure from previous methods that we reported is the use of wavelet analysis for the determination of the breathing rate. This is a better approach than Fourier analysis, as breathing is a non-stationary process. Based on the largest scale experiment we conducted yet, the thermal imaging measurement appears to be in par with the existing clinical standard. Imaging-based breathing measurements may find wide applicability in sleep studies and neonate physiological monitoring due to their unobtrusive nature.

References

[1] F. H. Martini, W. C. Ober, C. W. Garrison, K. Welch, and R. T. Hutchings, *Fundamentals of Anatomy and Physiology*, ch. 23. Upper Saddle River, N.J.: Prentice Hall, 5th ed., 2001.

[2] Y. Zhang, "Quantitative measurement of radiation properties for opaque and semi-transparent greybodies," *Infrared Phys.*, vol. 30, no. 2, pp. 149–153, 1990.

[3] J. Lindemann, R. Leiacker, G. Rettinger, and T. Keck, "Nasal mucosal temperature during respiration," *Clin. Otolaryngol*, vol. 27, pp. 135–139, 2002.

[4] ADInstruments, 2205 Executive Circle, Colorado Springs, Colorado 80906, *http://www.adinstruments.com*, 2007.

[5] K. Storck, M. Karlsson, P. Ask, and D. Loyd, "Heat transfer evaluation of the nasal thermistor technique," *IEEE Transactions on Biomedical Engineering*, vol. 43, pp. 1187 – 1191, Dec. 1996.

[6] E. Greneker, "Radar sensing of heartbeat and respiration at a distance with security applications," in *Proceedings of SPIE, Radar Sensor Technology II*, vol. 3066, (Orlando, Florida), pp. 22–27, April 1997.

[7] M. Garbey, A. Merla, and I. Pavlidis, "Estimation of blood flow speed and vessel location from thermal video," in *Proceedings of the IEEE Computer Society Conference on Computer Vision and Pattern Recognition*, vol. 1, (Washington, DC), pp. 356 – 363, June 27 - July 2 2004.

[8] N. Sun, I. Pavlidis, M. Garbey, and J. Fei, "Harvesting the thermal cardiac pulse signal," in *International Society and Conference Series on Medical Image Computing and Computer-Assisted Intervention (MICCAI)*, vol. 4191 of *Lecture Notes in Computer Science*, (Copenhagen, Denmark), pp. 569 – 576, Springer, 1-6 Oct 2006.

[9] R. Murthy, I. Pavlidis, and P. Tsiamyrtzis, "Touchless monitoring of breathing function," in *Proceedings of the 26th Annual International Conference IEEE Engineering in Medicine and Biology Society*, vol. 2, (San Fransisco, CA), pp. 1196 – 1199, September 2004.

[10] J. Fei, Z. Zhu, and I. Pavlidis, "Imaging breathing rate in the co_2 absorption band," in *Proceedings of the 27th Annual International Conference IEEE Engineering in Medicine and Biology Society*, (Shanghai, China), pp. 700–705, September 1-4 2005.

[11] I. Pavlidis, "Continuous physiological monitoring," in *Proceedings of the 25th Annual International Conference of the IEEE Engineering in Medicine and Biology Society*, vol. 2, (Cancun, Mexico), pp. 1084 – 1087, September 17-21 2003.

[12] J. Dowdall, I. Pavlidis, and P. Tsiamyrtzis, "Coalitional tracking," *Computer Vision and Image Understanding*, vol. 106, pp. 205–219, May-June 2007.

[13] M. Isard and A. Blake, "CONDENSATION - conditional density propagation for visual tracking," *International Journal of Computer Vision*, vol. 19, no. 1, pp. 5 – 28, 1998.

[14] I. Daubechies, *Ten lectures on wavelets*. SIAM, 1992.

[15] FLIR Systems, 25 Esquire Road, North Billerica, Massachussetts 01862, *http://www.flir.com*, 2007.